ACS APPLIED MATERIALS & INTERFACES

www.acsami.org

Research Article

Bioengineered Polymer Nanobeads for Isolation and Electrochemical Detection of Cancer Biomarkers

Narshone Soda,[#] Zennia Jean Gonzaga,[#] Shuxiong Chen, Kevin M. Koo, Nam-Trung Nguyen, Muhammad J. A. Shiddiky,[*] and Bernd H. A. Rehm[*]

Cite This: *ACS Appl. Mater. Interfaces* 2021, 13, 31418–31430

Read Online

ACCESS | Metrics & More | Article Recommendations | Supporting Information

ABSTRACT: Early sensitive diagnosis of cancer is critical for enhancing treatment success. We previously bioengineered multifunctional core–shell structures composed of a poly-3-hydroxybutyrate (PHB) core densely coated with protein functions for uses in bioseparation and immunodiagnostic applications. Here, we report bioengineering of *Escherichia coli* to self-assemble PHB inclusions that codisplay a ferritin-derived iron-binding peptide and the protein A-derived antibody-binding Z domain. The iron-binding peptide mediated surface coating with a ferrofluid imparting superparamagnetic properties, while the Z domain remained accessible for binding of cancer biomarker-specific antibodies. We demonstrated that these nanobeads can specifically bind biomarkers in complex mixtures, enabling efficient magnetic separation toward enhanced electrochemical detection of cancer biomarkers such as methylated DNA and exosomes from cancer cells. Our study revealed that superparamagnetic core–shell structures can be derived from biological self-assembly systems for uses in sensitive and specific electrochemical detection of cancer biomarkers, laying the foundation for engineering advanced nanomaterials for diverse diagnostic approaches.

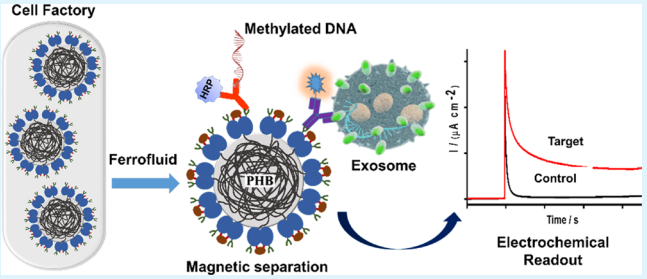

KEYWORDS: *poly-3-hydroxybutyrate, self-assembly, superparamagnetism, nanobeads, DNA methylation, exosomes, electrochemical biosensor*

1. INTRODUCTION

Material sciences have gained remarkable attention due to the continuous progress in controlled synthesis and processing of innovative materials within the nanometer scale. These nanomaterials have been applied in biosensing assays due to their unique properties exhibited at the nanoscale, which can substantially improve analytical specificity and sensitivity.[1,2] Biopolymers have increasingly attracted interest as advanced materials that can be engineered to exhibit unique advantageous properties for diagnostic application.[3,4] For biosensing, nanomaterials, such as carbon-/silica-based inorganic nanomaterials or paramagnetic iron oxide nanoparticles, have typically been utilized in biomolecule isolation to enable rapid, cost-effective, and high-throughput workflows.[5] Despite broad usage feasibility, nanomaterial manufacturing generally has limitations as they are often not amendable toward larger-scale industrial production. Additionally, the toxicity and environmental impact of these inorganic nanomaterials are considerable.[6]

Bioengineered polyhydroxybutyric acid (PHB) beads (~100–300 nm) are naturally synthesized and assembled inside cells of a wide range of bacteria and serve as a reserve material. Industrial microbial production hosts such as *Escherichia coli*[7,8] (*E. coli*) or *Bacillus megaterium*[9] were engineered to produce surface-functionalized PHB beads enabling low-cost manufacturing processes and the development of molecular tools to precision-engineer high-performance materials for uses such as in bioassays.[8,10−12] Bioengineered PHB nanobeads are core–shell structures where the core is made of semicrystalline hydrophobic PHB exhibiting unique thermal and mechanical properties while the surface is composed of covalently anchored proteins that can be engineered to densely present binding domains in a homogeneous orientation facilitating access to target molecules suitable for biosensing applications (Figure 1).[3,13,14] The self-assembly of PHB-anchored proteins translationally fused to protein functions during PHB synthesis enables the dense and oriented display of various protein functions on the surface for enhanced target capture and recognition.[14−16] The increased functional surface area of PHB nanobeads also allows for integration of inorganic binding peptides that mediate binding such as gold, silica,[10] cadmium,[17] and, as described in this study, iron oxide to convey additional physical properties such

Received: March 22, 2021
Accepted: June 14, 2021
Published: June 29, 2021

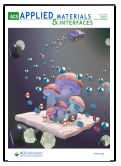

https://doi.org/10.1021/acsami.1c05355
ACS Appl. Mater. Interfaces 2021, 13, 31418–31430

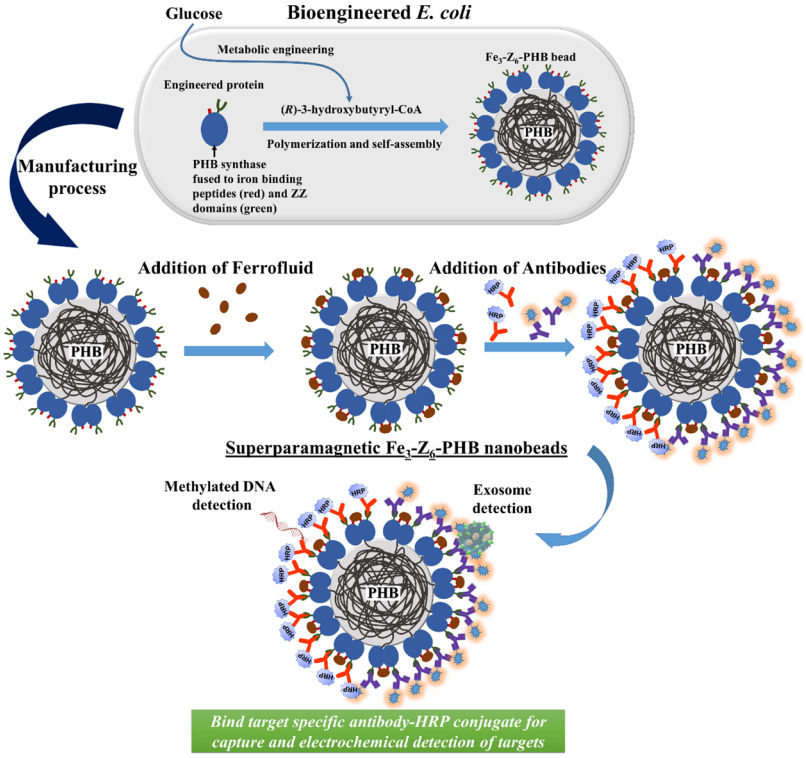

Figure 1. Schematic overview of the assembly of superparamagnetic PHB nanobeads. *E. coli* BL21 (DE3) was engineered to efficiently convert glucose into (*R*)-3-hydroxybutyryl-CoA, the PHB precursor. The PHB synthase fusion protein was overproduced at the same time and catalyzed polymerization of (*R*)-3-hydroxybutyryl-CoA to PHB while generating a surface coat that displays iron-binding peptides and IgG-binding ZZ domains. These core−shell structures were manufactured and processed into superparamagnetic nanobeads using a ferrous fluid. Addition of various target-specific antibody−HRP conjugates enable specific sequestration of the targets from complex mixtures by magnetic separation followed by elution of the antibody-bound target and sensitive electrochemical detection.

as superparamagnetism. Here, we bioengineered *E. coli* to assemble PHB nanobeads that were able to specifically bind any antibody via its Fc domain and that could be processed into superparamagnetic nanobeads. Such nanobeads could be easily dispersed in solution and then retrieved using an external magnet.[18] In particular, we describe the use of such superparamagnetic PHB nanobeads as a promising tool for magnetic isolation and detection of target biomolecules present in complex biomatrices. We exemplified the functionality of superparamagnetic PHB nanobeads by demonstrating isolation and electrochemical detection of traditionally challenging biomarkers such as methylated DNA and exosomes.

DNA methylation is a covalent modification that occurs at the fifth carbon position of the pyrimidine ring of cytosines within cytosine-guanine (CpG) dinucleotides[19,20] and is one of the key epigenetic signatures that are essential for regulating cellular pathways.[21−23] In cancer, aberrant DNA methylation at CpG-rich regions is usually associated with long-term repression of gene expression. Thus, precise quantification of global DNA methylation levels in cells could serve as a useful cancer biomarker. To date, the gold standard detection method for DNA methylation is based on bisulfite treatment of methylated bases before analysis.[24,25] However, bisulfite treatment requires long assay duration, experienced lab personnel, and tedious workflows, therefore limiting its practical applicability in clinical settings. Hence, the development of alternative methods for rapid, simple, and cost-effective isolation and detection of global DNA methylation levels would be greatly useful.

Exosomes are nanometer-sized vesicles (30−150 nm) generated in the endosomal compartment and are released by virtually every cell type in the body.[26] Exosomes have been shown to be key mediators of cell-to-cell communication, delivering a distinct cargo of lipids, proteins, and nucleic acids that reflect their cell of origin.[27] Owing to their composition, easy accessibility, and ability to represent their parental cells, exosomes recently attracted increasing interest as promising biomarkers for liquid biopsies.[28] Exosomes exist in all body fluids including blood, urine, and saliva and are generated by most of the normal and pathological cells.[29] Thus, there is a need for development of accurate isolation and detection techniques of disease-specific exosomes.

To date, several isolation and enrichment technologies have been developed for exosomes such as immunoaffinity capture-based methods, ultracentrifugation, and polymer precipitation. Immunoaffinity-based methods provide highly specific strategies to isolate exosomes via the affinity interactions between exosomal proteins and their specific antibodies or receptors and their cognate ligands. However, the efficiency of these methods is greatly dependent on the selection of an appropriate membrane marker and respective antibodies or ligand interaction. Although ultracentrifugation methods are inexpensive and rapid, the filter poles of the membranes often trap vesicles, which subsequently reduces the exosome yield. Polymer precipitation methods offer relatively simple isolation with no specialized instrumentation required. However, the specificity can be affected by the coseparation of impurities and polymer molecules. Thus, developing a sensitive single-step method that can rapidly isolate and subsequently detect

https://doi.org/10.1021/acsami.1c05355
ACS Appl. Mater. Interfaces 2021, 13, 31418−31430

exosomes would be transformative in the clinical research of exosomal biomarkers.

In this study, we report the bioengineering of *E. coli* to assemble antibody-bound PHB nanobeads that can be processed to become superparamagnetic for electrochemical quantification of global DNA methylation and cancer-derived exosomes. Superparamagnetic PHB nanobeads exhibited specific binding to antibodies and superparamagnetic properties, enabling magnetic separation of methylated DNA and exosomes for specific recognition via coupled peroxidase-mediated electrochemical reactions. The size and surface properties of the bioengineered PHB nanobeads were characterized to assess their suitability for capture, isolation, and purification of methylated DNA targets and exosomes from ovarian cancer cells. Post-purification, the methylated DNA targets and exosomes were directly adsorbed onto a screen-printed gold electrode (SPE-Au) surface. The methylated DNA targets and exosomes were then analytically quantified using a catalytic redox cycling system of hydrogen peroxide/horseradish peroxidase/hydroquinone (H_2O_2/HRP/HQ).

2. EXPERIMENTAL SECTION

2.1. Reagents and Chemicals. All chemicals and reagents were of analytical grade and obtained from Sigma-Aldrich (Sydney, NSW, Australia). UltraPure DNase/RNase-free distilled water was purchased from Invitrogen (Carlsbad, CA, USA). An SPE-Au with a three-electrode system was purchased from Dropsens (Llanera, Asturias, Spain). In the three-electrode system, working (diameter = 4 mm), counter, and reference electrodes were gold, platinum, and silver-modified electrodes, respectively. Hydroquinone and hydrogen peroxide solution were purchased from Thermo Fisher Scientific Australia Pty Ltd. (Scoresby, VIC, Australia). A 5-methylcytosine (5mC) antibody and a horseradish peroxidase (HRP) conjugation kit were purchased from Abcam (Melbourne, VIC, Australia).

2.2. Preparation and Characterization of PHB Nanobeads.

2.2.1. Bacterial Strains, Plasmids, Primers, and Cultivation Conditions. Bacterial strains, plasmids, and primers used in this study are listed in Table S1. *E. coli* XL1-Blue was grown at 37 °C in Luria−Bertani (LB) containing 100 μg/mL ampicillin (Amp) and was used for plasmid propagation. PHB nanobeads were produced in a recombinant *E. coli* BL21 (DE3) strain harboring the respective plasmids in LB media supplemented with 1% (w/v) glucose, 100 μg/mL Amp, and 50 μg/mL chloramphenicol (Cm).

2.2.2. Plasmid Construction Mediating PHB Production Displaying ZZ and Iron (Fe)-Binding Domains. Three plasmids were used for PHB production: (1) pET14b_PHB, (2) pET14b_Z_6-PHB, and (3) pET14b_Fe_3-Z_6-PHB. General cloning procedures and isolation of DNA were performed as described elsewhere.[30] The gene-encoding Z_4 and Fe_3 (three repeats of the iron-binding peptide derived from ferritin) were synthesized by Genscript Corporation (USA) employing codon optimization for *E. coli* and were cloned into pET14b_PHB-Z_2[31] and pET14b_Z_6-PHB vectors, respectively, generating the final plasmids pET14b_Z_6-PHB and pET14b_Fe_3-Z_6-PHB. The plasmid sequences were confirmed by DNA sequencing using T7 promoter and T7 terminator primers (Table S1).

2.2.3. PHB Nanobead Production, Isolation, and Purification. *E. coli* BL21 (DE3) harboring the pMCS69 plasmid was transformed with pET14b_PHB (plain PHB nanobeads as a negative control), pET14b_Z_6-PHB (PHB nanobeads displaying ZZ domains as a positive control), and pET14b_Fe_3-Z_6-PHB (PHB nanobeads displaying ZZ domains and Fe-binding peptides). The pMCS69 plasmid comprises the genes encoding PhaA and PhaB enzymes of *Ralstonia eutropha* that enables the production of the precursor *R*-3-hydroxybutyrate-coenzyme A mediating PHB production.[32] The recombinant *E. coli* BL21 (DE3) strains were grown at 37 °C until optical density at 600 nm (OD_{600}) reached 0.5−0.8 and subsequently induced by addition of 1 mM isopropyl-β-D-thiogalactopyranoside (IPTG) (Goldbio, USA). The culture was incubated further for 48 h at 25 °C. The cells were harvested, and PHB nanobeads were isolated and purified as previously described.[33] PHB nanobeads were stored in 10 mM Tris-HCl (pH 7.5) with 20% ethanol.

2.2.4. PHB Nanobead Characterization. Nile red staining and fluorescence microscopy (FM) were used to detect and analyze the cells producing PHB nanobeads as previously described.[34] The morphology of the PHB nanobeads was observed by transmission electron microscopy (TEM) and scanning electron microscopy (SEM). The preparation of samples for TEM followed procedures previously described.[15] Prior to SEM analyses and imaging, the PHB nanobeads were subjected to immobilization and drying and sputter-coated with an ultrathin layer of platinum in an argon atmosphere to make them electronically conductive. The average particle size and zeta potential of the purified PHB nanobeads were determined by dynamic light scattering (DLS) at room temperature, using a Zetasizer Nano ZS (Malvern Panalytical, Malvern, U.K.). The nanobeads were diluted prior to size measurement to avoid multiple scattering effects. All measurements were performed in triplicate. To analyze the PHB content of the whole cells and purified PHB nanobeads, the lyophilized samples were processed and subjected to crotonic analysis as previously described.[35] The superparamagnetism activity of the Fe_3-Z_6-PHB nanobeads was analyzed by vibrating sample magnetometer (VSM) measurements at room temperature as previously described.[36]

Fusion proteins displayed on the surface of PHB nanobeads were denatured using reducing conditions and sodium dodecyl sulfate at 95 °C, which mediated quantitative release from the PHB nanobeads enabling analysis by sodium dodecyl sulfate-polyacrylamide gel electrophoresis (SDS-PAGE) as previously described.[33] Densitometry was used to analyze protein concentration using bovine serum albumin (BSA) standards as previously described.[37] To confirm the identity of the fusion proteins, Coomassie-stained protein bands of interest were excised and processed for liquid chromatography-tandem quad time-of-flight mass spectrometry (MS-Q-TOF) as previously described.[15]

2.2.5. Functionality of PHB Nanobeads Displaying ZZ Domains. An IgG-binding capacity assay was used to assess the functionality of Z_6-PHB and Fe_3-Z_6-PHB nanobeads as previously described.[31] PHB nanobeads of 40−60 mg wet weight were used and washed twice with 1× PBS buffer (pH 7.5) by pipetting. Samples were centrifuged at 6000*g* for 4 min between each wash in order to remove ethanol. All samples were resuspended in 500 μL of 1× PBS buffer, and 5 mg of human IgG (Sigma-Aldrich, USA) was added to each sample and incubated at 25 °C for 30 min with agitation to allow IgG binding to occur. After incubation, the tubes were centrifuged at 6000*g* for 4 min, and the unbound fraction of IgG in supernatants was aliquoted and analyzed. The sediment was washed three times with 1× PBS buffer by pipetting subsequently followed by centrifugation at 6000*g* for 4 min between each wash. Bound IgG from PHB nanobeads was eluted by resuspending the sediment in 0.5 mL of 50 mM glycine (pH 2.7) and incubated at room temperature for 5 min with agitation. Then, the samples were centrifuged at 16,200*g* for 4 min, and the eluted IgG in supernatants was neutralized by adding 10 μL of 1 M K_2HPO_4 and analyzed. Protein concentrations were analyzed using the Bradford assay.

2.2.6. Functionality of Superparamagnetic PHB Nanobeads. PHB nanobeads of 40−60 mg wet weight were used and washed twice with 1× PBS buffer (pH 7.5) by pipetting. Samples were centrifuged at 6000*g* for 4 min between each wash in order to remove ethanol. All samples were resuspended in 500 μL of 1× PBS buffer, and 1/100 dilution of a commercial ferrofluid (Magron, Republic of Korea) was added and incubated at 25 °C for 30 min with agitation. After incubation, the tubes were centrifuged at 6000*g* for 4 min, and the supernatant was discarded. The magnetized nanobeads (pellet) were washed three times with 1× PBS buffer (pH 7.5) by incubating for 2 min on a magnetic rack. After washing, all the samples were resuspended in 500 μL of 1× PBS buffer, and 5 mg of human IgG (Sigma-Aldrich, USA) was added to each sample and incubated at 25

https://doi.org/10.1021/acsami.1c05355
ACS Appl. Mater. Interfaces 2021, 13, 31418−31430

°C for 30 min with agitation to allow IgG binding to occur. The tubes were incubated on a magnetic rack for 2 min, and supernatants (unbound IgG fraction) were aliquoted and analyzed. The sediments were washed three times with 1× PBS buffer by incubating on a magnetic rack for 2 min. Bound IgG was eluted by resuspending the sediments in 0.5 mL of 50 mM glycine (pH 2.7) and incubated at room temperature for 5 min with agitation. Then, the samples were centrifuged at 16,200*g* for 4 min, and the eluted IgG in supernatants was neutralized by adding 10 μL of 1 M K_2HPO_4 and analyzed. Protein concentrations were analyzed using the Bradford assay.

2.3. HRP Conjugation with 5mC and CD9 Antibodies. The HRP enzyme was conjugated to the antibodies using the HRP conjugation kit (Abcam) according to the manufacturer's instructions. Briefly, 1 μL of a modifier reagent was mixed gently with 10 μL of antibodies (1 mg mL). Then, the modifier-mixed antibodies were added directly to the lyophilized HRP mix and resuspended two times by pipetting. The complexes were then kept overnight in the dark at room temperature to facilitate the conjugation of antibodies with HRP. After the incubation, 1.0 μL of a quencher reagent was mixed gently to the solution. The conjugated antibody solutions were stored at 4 °C until further use in the study.

2.4. Biotinylation of the CA-125 Antibody. The CA125 monoclonal antibody was biotinylated using a biotin (type B) conjugation kit (Abcam) following the manufacturer's guidelines. Briefly, 10 μL of a modifier reagent was mixed gently with 100 μL of the antibody (0.1 mg/mL). Then, the antibody−modifier mixture was added directly into the lyophilized biotin material and resuspended several times by pipetting. The complex was then incubated for 15 min in the dark at room temperature to allow the conjugation of the antibody with biotin. After incubation, 10 μL of the quencher reagent was added to the solution and mixed gently, and then, the conjugated antibody was ready for use.

2.5. Preparation of DNA from Ovarian Cell Lines. An RPMI-1640 growth medium (Life Technologies, Australia) supplemented with 10% fetal bovine serum (Life Technologies, Australia) and 1% penicillin/streptomycin (Life Technologies) was used to culture ovarian cancer cell lines (SKOV3 and OVCAR3) and a noncancerous cell line (Met-5A). This was performed in a humidified incubator with a 5% CO_2 flow at 37 °C. All cells were harvested by a standard trypsinization protocol after they reached 70−80% confluence. Briefly, cells were washed with 3 mL of HBSS (Gibco) to remove enzyme inhibitors followed by 1−2 mL of TryPLe (Gibco) and incubation for 3 min at 37 °C. To neutralize the trypsin activity, 3−6 mL of cell culture media was added followed by centrifugation for 5 min at 2500 rpm. A cell pellet was collected for DNA extraction and stored at −20 °C until further processing. A DNeasy Blood & Tissue Kit (Qiagen, Australia) was used to extract DNA, and the concentration was quantified using a SPECTROstar Nano microplate reader (BMG Labtech) operated by MARS data analysis software.

2.6. Cell Culture and Isolation of Exosomes. The ovarian cancer cell line OVCAR3 and the noncancerous cell line MeT-5A were cultured in 75 cm^2 flasks (Life Technologies, Australia) at 37 °C and 5% CO_2 in an RPMI-1640 growth medium (Life Technologies, Australia) supplemented with 10% fetal bovine serum (Life Technologies, Australia) and 1% penicillin/streptomycin (Life Technologies). The cell culture medium containing exosomes was collected after 72 h. Exosomes were isolated using a total exosome isolation reagent (Life Technologies) as per the manufacturer's guidelines. Briefly, the supernatant was transferred to a new tube, and the isolation reagent was added to the tube in a 2:1 ratio. The samples were incubated overnight at 4 °C and centrifuged at 10,000*g* for 1 h to obtain exosome pellets. Exosome pellets were then resuspended in 50 μL of phosphate-buffered saline (PBS; 10 mM, pH 7.4) and stored at −20 °C for further use.

2.7. Determination of the Surface Area of the Electrodes. Prior to DNA adsorption, the effective working area of each electrode was measured as a function of the scan rate under cyclic voltammetric conditions for the one-electron reduction of $[Fe(CN)_6]^{3-}$ using the Randles−Ševčík equation

$$i_p = (269 \times 10^5) n^{3/2} A D^{1/2} C \nu^{1/2} \quad (1)$$

where i_p is the peak current (A), n is the number of electrons transferred ($Fe^{3+} \rightarrow Fe^{2+}$, $n = 1$), A is the effective area of the electrode (cm^2), D is the diffusion coefficient of $[Fe(CN)_6]^{3-}$ (taken to be 7.60×10^{-5} cm^2 s^{-1}), C is the concentration (mol cm^{-3}), and ν is the scan rate (V s^{-1}).

2.8. Magnetization and IgG Binding of PHB Nanobeads. About 20−40 mg wet weight of PHB nanobeads for each sample was measured in a 1.5 mL microfuge tube. All nanobeads were washed twice with 1× PBS buffer by pipetting to remove stored ethanol. Samples were centrifuged at 6000*g* for 4 min (Heraeus Pico 17, Thermo Scientific) after each wash. A freshly prepared commercial ferrofluid (Magron, Republic of Korea) was mixed with the plain nanobeads at a ratio of 20:1 (volume, μL; wet weight, mg) and then incubated at room temperature for half an hour with agitation. After incubation, the tubes were centrifuged at 6000*g* for 4 min, and the supernatant was discarded. The pellets (superparamagnetic nanobeads) were washed three times with 1× PBS buffer. A 5mC−HRP or CD9−HRP conjugate was added to ferrofluid-functionalized PHB nanobeads and incubated for 30 min with agitation followed by gentle washing three times on a magnetic rack, and aliquots of the supernatant (unbound antibody fraction) were taken for further analysis.

2.9. DNA Preparation, Magnetic Separation, and Adsorption on the Electrode. A CpGenome human methylated and nonmethylated DNA standard set Jurkat DNA (100% methylated) was purchased from Merck (Sydney, NSW, Australia). Whole genome amplification (WGA) DNA was generated using the protocol of a REPLI-g whole genome amplification kit (Qiagen).

The 5mC−HRP magnetic bead complexes were then dispersed into a denatured DNA sample, and 5mC antibodies specifically recognize and bind the DNA on the methylated CpG sites. The captured methylated DNA was magnetically isolated and purified by lowering the pH of glycine and centrifuging at 16,200*g* for 4 min. The isolated DNA complex was directly adsorbed on an SPE-Au via DNA−gold affinity interaction[38] and electrochemically quantified by chronoamperometry using a H_2O_2/HRP/HQ system. A CH1040C potentiostat (CH Instruments, TX, USA) was used to perform electrochemical measurements. Amperometric measurements in HQ solution were made at −0.2 V vs a Ag pseudo-reference electrode. Once the background current stabilized, 10 μL of H_2O_2 solution was added, and the generated current was recorded until the steady-state current was reached. The amperometric measurements given through the whole experiments correspond to the difference between the steady-state and the background currents and are the average of at least three replicates.

2.10. Exosome Isolation Using PHB Nanobeads. For exosomes analysis extracted from the cell lines, 10 μL of isolated exosomes of varying concentrations was mixed with 10 μL of CD9-functionalized magnetic nanobeads. The mixture was placed on a thermomixer at 300 rpm for 1 h at room temperature to allow the antibody to capture exosome targets. After this step, the exosome-attached magnetic beads were isolated with a magnet and washed three times with PBS buffer. The sediment was resuspended in 10 μL of glycine (pH 2.7) and incubated for 5 min with agitation (500 rpm). This was followed by centrifugation at 16200*g* for 4 min to elute the target bound to CD9−HRP. Immediately, 2 μL of K_2HPO_4 was added to neutralize the pH.

2.11. Electrochemical Detection of Exosomes. Five microliters (100 ng/mL) of the biotinylated CA125 antibody was first incubated on a streptavidin-modified SPCE (SPCE-STR) surface for 30 min. After the incubation, the electrode surface was washed with PBS buffer 3 times to remove loosely attached or unattached CA125 antibodies. To avoid nonspecific binding of exosomes or any other biomolecules, the electrode surface was then incubated with 1% bovine serum albumin (BSA) solution (blocking agent) for 20 min. Isolated CD9/HRP/exosome conjugates (5 μL) were then added to the SPCE-STR surface and incubated for 1 h on a mixer (300 rpm) at

https://doi.org/10.1021/acsami.1c05355
ACS Appl. Mater. Interfaces 2021, 13, 31418−31430

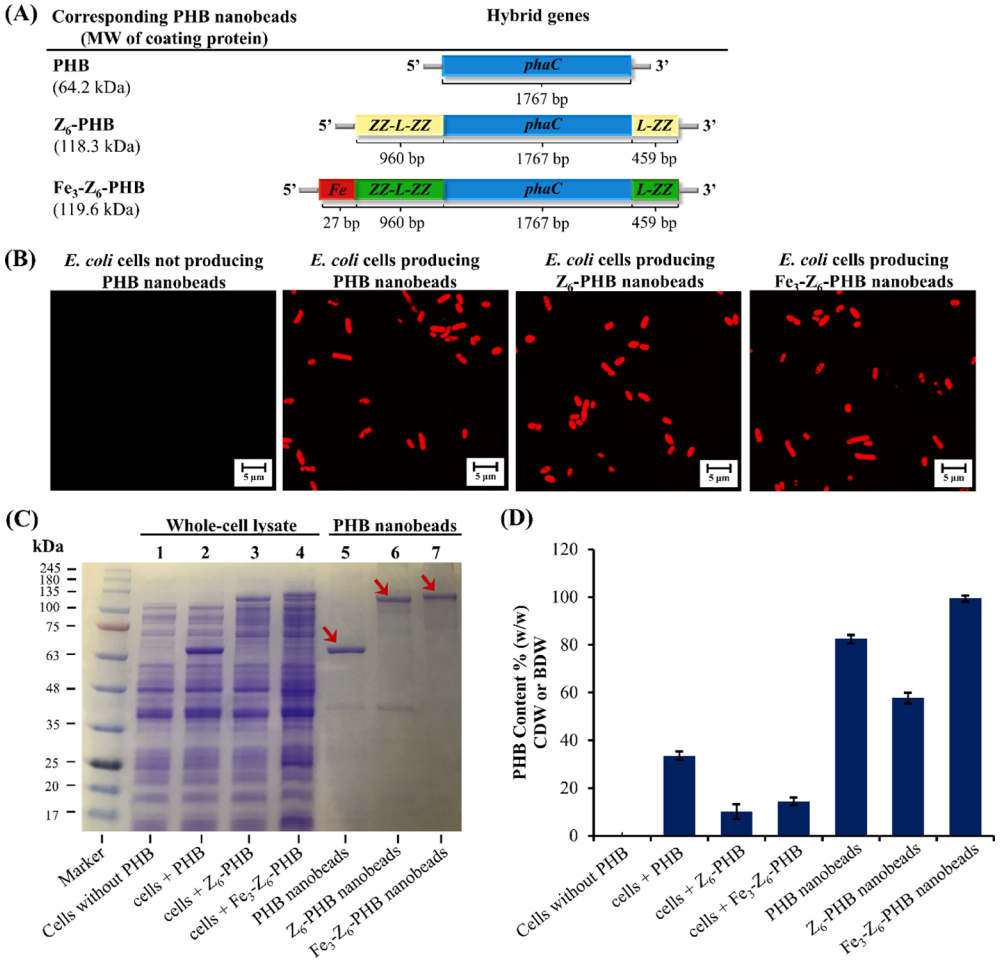

Figure 2. Production and biochemical characterization of various PHB nanobeads. (A) Schematic overview of hybrid genes encoding fusion proteins for the production of PHB, Z_6-PHB, and Fe_3-Z_6-PHB nanobeads. MW, molecular weight. (B) Nile red staining and fluorescence microscopy of recombinant *E. coli* BL21 (DE3) cells (pMCS69) harboring various plasmids. (C) Protein profile analysis of recombinant *E. coli* cells (pMCS69) and purified PHB nanobeads by SDS-PAGE with Coomassie blue staining. Proteins were encoded by hybrid genes depicted in (A). The protein bands of PHB (64.2 kDa), Z_6-PHB (118.3 kDa), and Fe_3-Z_6-PHB (119.6 kDa) proteins are indicated by red arrows. MS-Q-TOF was used to confirm the fusion protein identity (Table S2). (D) PHB content analysis of whole cells and purified PHB nanobeads shown as percentage of CDW or BDW (CDW, cellular dry weight; BDW, polyester nanobead dry weight).

room temperature. The complete sandwich assay was monitored using the redox cycling of a H_2O_2/HRP/HQ system.

2.12. Statistical Analysis. IgG-binding capacity of PHB nanobeads was analyzed using one-way ANOVA with statistical significance ($p < 0.05$) indicated by letter-based representation of pairwise comparison between groups using Tukey's post hoc test. Each data point of measurement represents the mean ± the standard error of the mean. All measurements were conducted in triplicate.

3. RESULTS

3.1. Bioengineering of *E. coli* and Production of Superparamagnetic PHB Nanobeads. The engineering of superparamagnetic PHB nanobeads that specifically bind antibodies for target detection holds the promise of an attractive high-performance nanomaterial. This is due to assembly-driven, dense, and homogeneous functional orientation of binding sites (e.g., to bind specific antibodies) for maximum surface interaction ideally suited for sequestration and detection of the target of interest.[14] Furthermore, these nanobeads are stable up to 85 °C and can be stored for several months to years.[39]

We here describe the bioengineering and production of PHB nanobeads via a low-cost process that avoids sophisticated instrumentation and separation techniques. PHB naturally serves as carbon and energy storage for bacteria during nutrient imbalance. PHB synthase (PhaC) is the key enzyme for the formation of spherical insoluble PHB nanobeads within bacterial cells.[40] *E. coli* does not naturally produce PHB but can be genetically engineered to enable PHB nanobead production.[31] The production of PHB nanobeads is scalable as it can tap into industrial large-scale fermentation processes established for *E. coli* to enable high-yield production of core–shell nanobeads densely coated with proteins/peptides of interest.[41]

Previous studies have shown PHB nanobeads to be effective and efficient in bioseparation applications. For instance, PHB nanobeads displaying the immunoglobulin G (IgG)-binding ZZ domain of protein A from *Staphylococcus aureus* (ZZ-PHB nanobeads) produced in recombinant *E. coli* had comparable IgG-binding capacity and purification abilities to the commercial protein A sepharose.[14] In addition, PHB nanobeads displaying ZZ domains that were produced in engineered *Lactococcus lactis* or *Bacillus megaterium* also showed high IgG-binding capacity, suggesting that different

https://doi.org/10.1021/acsami.1c05355
ACS Appl. Mater. Interfaces 2021, 13, 31418−31430

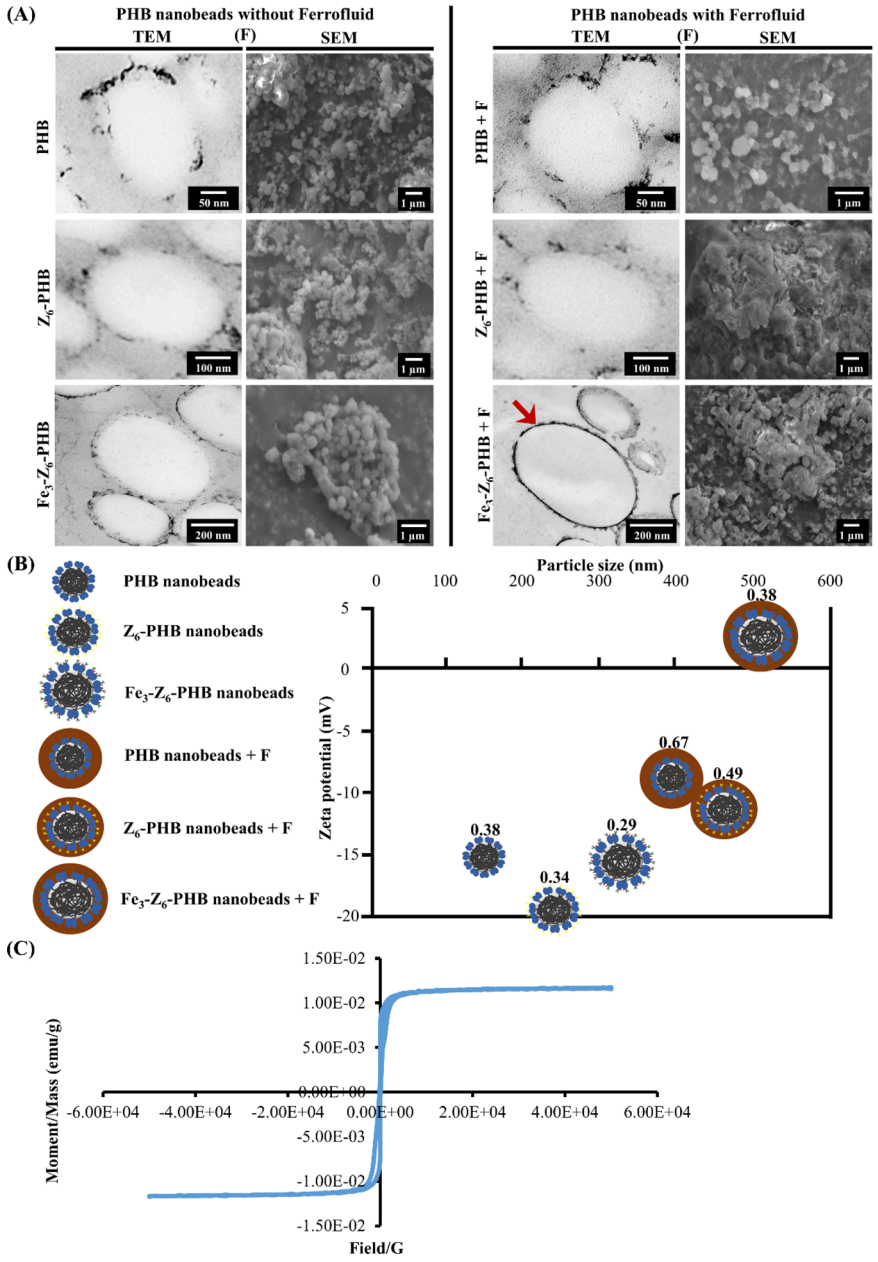

Figure 3. Physical characterization of various PHB nanobeads with and without a ferrofluid. (A) TEM and SEM images. A representative granule is shown in TEM images. Whole TEM images are shown in Figure S2. (B) Particle sizes and zeta potentials of the purified PHB nanobeads before and after addition of a ferrofluid. The particle size and zeta potential of each type of PHB nanobead were measured in triplicates using a Zetasizer Nano ZS. Each data point of measurement represents the mean ± the standard error of the mean. Polydispersity indices are shown above the nanobeads. Values are in Table S3. F, ferrofluid. (C) Vibrating sample magnetometer (VSM) result showing the magnetization curve of the Fe_3-Z_6-PHB nanobeads with a ferrofluid at 37 °C. G, Gauss.

hosts could be used for different applications of PHB nanobeads.[9,42]

Figure 1 shows an overview of the production, isolation, and processing of superparamagnetic PHB nanobeads. In the presence of an excess carbon source such as glucose, recombinant *E. coli* can overexpress the integrated hybrid genes *3xFe-ZZ-L-ZZ-phaC-L-ZZ* (superparamagnetic Fe_3-Z_6-PHB nanobead production), *ZZ-L-ZZ-phaC-L-ZZ* (Z_6-PHB nanobead positive control), and *phaC* (PHB nanobead negative control) within the cells. This overexpression mediates assembly of PHB nanobeads densely coated with the respective fusion proteins or only PHB nanobeads, which can be isolated through mechanical cell disruption and purified using high pH and detergent washes. In this study, ZZ domains and Fe-binding peptides were bioengineered for codisplay on the surface of the PHB nanobeads (Fe_3-Z_6-PHB) and processed with iron oxide to become superparamagnetic for separation and detection of methylated DNA targets and exosomes. Although the bioengineered Fe_3-Z_6-PHB nanobeads are not naturally superparamagnetic, magnetism can be achieved when Fe-binding peptides on the bead surfaces sequester iron oxide in a ferrofluid in a magnetic field (Figure 1).[43]

3.2. Characterization of PHB Nanobeads. As shown in Figure 2A, three types of PHB nanobeads were produced in this study: (1) PHB nanobeads (plain nanobeads as a negative

https://doi.org/10.1021/acsami.1c05355
ACS Appl. Mater. Interfaces 2021, 13, 31418−31430

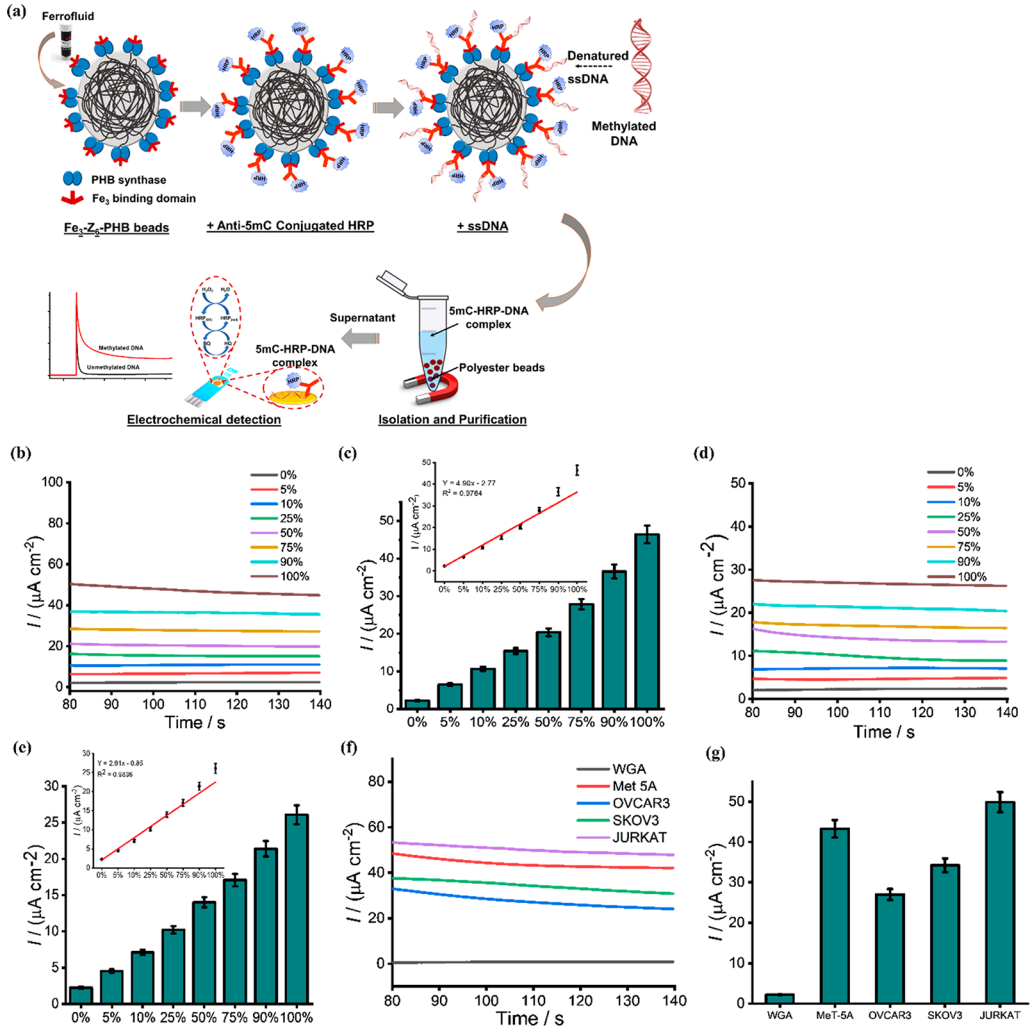

Figure 4. Superparamagnetic Fe_3-Z_6-PHB nanobeads for isolation and detection of methylated DNA targets. (A) Schematic representation of DNA methylation assay using superparamagnetic Fe_3-Z_6-PHB nanobeads. Methylated DNA targets (top, right) are captured and isolated magnetically and adsorbed directly onto a bare SPE-Au electrode surface (bottom). The amount of methylated DNA targets is analyzed by chronoamperometry using a H_2O_2/HRP/HQ catalytic redox cycling system (bottom, left). (B,C) Electrochemical detection of methylated DNA in a buffer sequestered by engineered superparamagnetic PHB nanobeads. (B) Current density responses corresponding to different % methylated DNA in a buffer. (C) Corresponding current density responses for each designated % methylated DNA. Inset, calibration plot showing linear % DNA methylation–current density relationship. (D,E) Electrochemical detection of methylated DNA in human plasma sequestered by engineered superparamagnetic PHB nanobeads. (D) Current density responses corresponding to different % methylated DNA in human plasma as a function of time. (E) Corresponding current density responses for each designated % methylated DNA. Inset, calibration plot showing linear % DNA methylation–current density relationship. (F,G) Comparative analysis of methylated DNA extracted from ovarian cancer cell lines and a normal cell line. (F) Amperometric response for different cell lines and (G) corresponding bar diagram representing current density comparison between different cell lines. Each data point represents the average of three repeat trails, and error bars represent the standard deviation of measurements (%RSD = <5%, for n = 3).

control), (2) Z_6-PHB nanobeads (PHB nanobeads with ZZ binding domains as a positive control for antibody binding), and (3) Fe_3-Z_6-PHB nanobeads (superparamagnetic nanobeads with ZZ binding domains and Fe-binding peptides). To detect and analyze the PHB nanobead-producing cells, lipophilic staining with a fluorescent dye Nile red and fluorescence microscopy (FM) were performed (Figure 2B). Fluorescent foci in whole *E. coli* cells producing PHB, Z_6-PHB, and Fe_3-Z_6-PHB were indicative of PHB production and a PHB synthase enzyme functionality. As expected, the negative *E. coli* control cells harboring empty plasmids did not show fluorescence. The protein profiles of the whole-cell lysate and purified nanobeads were analyzed by SDS-PAGE to show the production of full-length fusion proteins (Figure 2C). Dominating protein bands were observed and corresponded to the theoretical molecular weights of PHB (64.2 kDa), Z_6-PHB (118.3 kDa), and Fe_3-Z_6-PHB (119.6 kDa), thus indicating successful bioengineering of the various PHB nanobeads. Protein concentration was measured by densitometry using bovine serum albumin (BSA) standards. Productivity was assessed as the purified PHB nanobead mass yield over biomass of the bacterial production host in an unoptimized batch fermentation process. Yield percentages of 5 and 19% for Z_6-PHB and Fe_3-Z_6-PHB, respectively, suggested that the resin could be cost-effectively produced in industrial processes (Figure S1). Coating protein density was measured by determining the ratio of the Z fusion protein mass over PHB nanobead mass by SDS-PAGE combined with

https://doi.org/10.1021/acsami.1c05355
ACS Appl. Mater. Interfaces 2021, 13, 31418−31430

densitometry, and results suggest a dense coating with proteins, i.e., the Z domain and the iron-binding peptide (Figure S1). Protein identity was confirmed by liquid chromatography-tandem quad time-of-flight mass spectrometry (MS-Q-TOF) for detection of tryptic peptides (Table S2). Also, the PHB composition and quantity were confirmed by acid hydrolysis and detection of crotonic acid. The PHB content of whole cells and the purified nanobeads is shown in Figure 2D.[35]

Electron microscopy analysis of PHB nanobeads with and without the addition of a ferrofluid was done for morphology analysis (Figure 3A). Transmission electron microscopy (TEM) images confirmed the spherical shape of PHB nanobeads.[41,44] As previously observed, PHB nanobeads are polydisperse as seen in TEM images and depicted by varying bead sizes within the same sample (Figure S2).[33,44] In addition, imaging of the Fe_3-Z_6- PHB nanobeads after processing with a ferrofluid confirms the binding of iron oxide to the Fe-binding sites as shown by a thicker electron dense layer surrounding the nanobeads (red arrow) and proposed to contribute to their superparamagnetic properties. Furthermore, TEM and scanning electron microscopy (SEM) images showed the intact and generally spherical morphology of the purified nanobeads. Further physical characterization of PHB nanobeads such as particle size and zeta potential measurements revealed that the particle sizes of PHB nanobeads ranged between 151 and 324 nm (Figure 3B and Table S3) resembling the size distribution of previous reports,[14,41] while the negative zeta potential indicated an anionic surface charge.[15] The addition of a ferrofluid increased the particle size range to 405−504 nm. The negative zeta potentials of PHB nanobeads before the addition of a ferrofluid (i.e., the negative surface charge) were expected due to the theoretical isoelectric point (pI) of the proteins coating the nanobeads (theoretical pI values of PHB, Z_6-PHB, and Fe_3-Z_6-PHB are 6.08, 5.66, and 6.18, respectively). The addition of a ferrofluid made the zeta potential shift slightly to positive surface charge. A magnetic hysteresis curve of Fe_3-Z_6-PHB nanobeads with a ferrofluid was obtained by using a vibrating sample magnetometer (VSM) at 37 °C (Figure 3C). Remanence and coercivity were not observed in the hysteresis curve, thereby showing superparamagnetism properties.[36]

An IgG-binding assay was performed to confirm the functionality of ZZ domains displayed on PHB nanobeads before and after the addition of a ferrofluid (Figure S3).[31] In Figure S3A, the negative control PHB nanobeads showed low background IgG binding, therefore confirming low unspecific human IgG binding. PHB nanobeads that were engineered to display ZZ domains (Z_6-PHB and Fe_3-Z_6-PHB nanobeads) showed 9-fold higher IgG binding, which confirmed the functionality of the ZZ domains attached to the PHB nanobeads. However, the IgG-binding ability was reduced by about 50% when nanobeads are magnetized by addition of a ferrofluid (Figure S3B). Presumably, the surface-bound iron occluded binding sites impacting on the IgG-binding capacity.

3.3. Use of PHB Nanobeads for Isolation and Detection of Methylated DNA Targets. Figure 4A depicts the principle of using superparamagnetic Fe_3-Z_6-PHB nanobeads in an electrochemical DNA methylation assay. We compared a ferrofluid with iron oxide for processing Fe_3-Z_6-PHB nanobeads in superparamagnetic nanomaterials. However, we observed that surface functionalization via a ferrofluid provided greater magnetism as compared to iron oxide. This is probably due to the colloidal nature and nanoscale size of the ferromagnetic nanoparticles in a ferrofluid. The surfactant component (oleic acid) in the ferrofluid also inhibits aggregation or agglomeration of the nanobeads. Bioengineered Fe_3-Z_6-PHB nanobeads were made superparamagnetic with a ferrofluid and subsequently used to bind 5mC−HRP antibody conjugates for specific binding and detection of the methylated DNA target.

In the following step, the 5mC−HRP superparamagnetic nanobead complexes were added and dispersed into samples containing methylated DNA targets. The 5mC antibodies specifically recognize and bind to methylated DNA. The methylated DNA targets were then magnetically isolated and purified by lowering the pH of the glycine buffer, which released the 5mC−HRP-bound methylated DNA into the soluble fraction, while empty nanobeads were separated via attraction to an external magnet. Lastly, the 5mC−HRP-bound methylated DNA targets were adsorbed onto an SPE-Au electrode surface via the DNA−gold affinity interaction and electrochemically quantified by using a H_2O_2/HRP/HQ catalytic redox cycling system. To evaluate the assay functionality, we investigated the assay performance in the presence and absence of methylated DNA sequences. Figure S4 showed a 19-fold current density response for methylated compared to the negative control (2.41 vs 47.0 μA cm^{-2}).

3.4. Analytical Detection Performance for DNA Methylation. Aberrant methylation patterns are characterized by a gradual increase in global methylation levels during cancer development and can be used to track cancer progression from initial to advanced stage carcinoma.[45] Cancer patient samples are often heterogeneous with different proportions of methylation levels in different cells. Thus, it would be useful to quantify global methylation levels in heterogeneous backgrounds.

We tested the detection performance of our superparamagnetic Fe_3-Z_6-PHB nanobead-based electrochemical assay for quantification of heterogeneous global methylation levels by mixing Jurkat (100% methylated) with WGA (0% methylated) in different methylation ratios (i.e., 0, 5, 10, 25, 50, 75, 90, and 100% methylated DNA). The current density responses obtained for various methylation levels showed a linear relationship between current density responses and the methylation percentages (Figure 4B,C). The calibration plot (inset) exhibited excellent linearity from 0 to 100% DNA methylation with a correlation coefficient (R^2) of 0.9784 (n = 3). The lowest detectable methylation level was estimated to be as low as 5% from the extrapolated current density axes. While comparable LODs have also been reported previously based on graphene−DNA[46] and gold−DNA[47] affinity interaction-based electrochemical assays for DNA methylation, the use of superparamagnetic Fe_3-Z_6-PHB nanobeads has removed the reliance on commercial magnetic nanobeads.

The use of Fe_3-Z_6-PHB nanobeads in this work has the advantage of being biologically assembled for dense and homogeneously oriented display of binding domains for enhanced surface interaction not only mediating favorable magnetic properties via interaction with a ferrofluid but also exhibiting a high binding capacity for an antibody conjugate for specific target detection (Figures S2 and S4). Furthermore, the use of the 5mC antibodies on the superparamagnetic PHB nanobeads allows rapid concentration of the methylated DNA targets on the electrode surface by using a magnet, which

https://doi.org/10.1021/acsami.1c05355
ACS Appl. Mater. Interfaces 2021, 13, 31418−31430

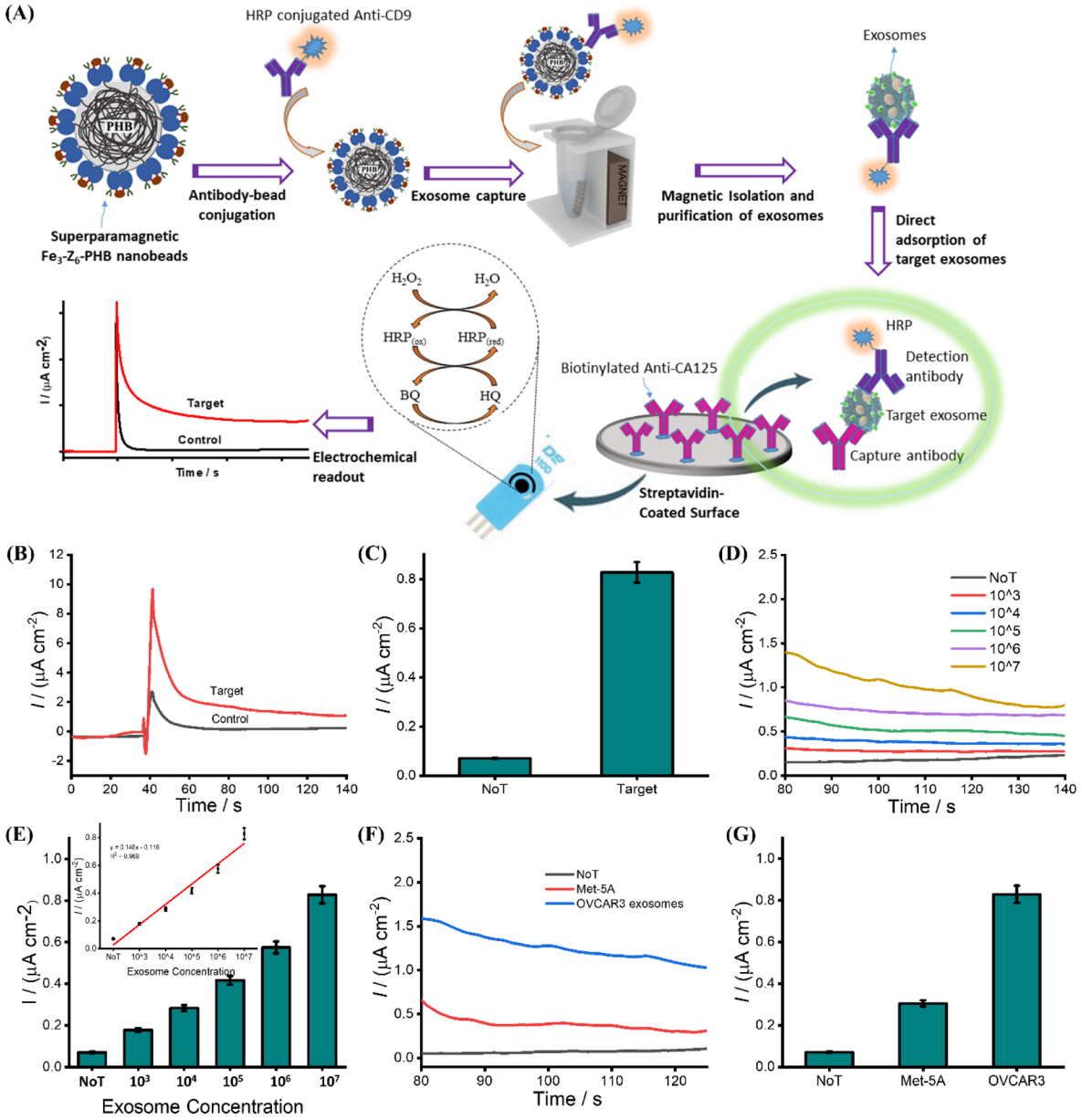

Figure 5. Superparamagnetic Fe_3-Z_6-PHB nanobeads for isolation and detection of exosomes. (A) Schematic representation of the assay for direct isolation and subsequent detection of exosomes using superparamagnetic PHB nanobeads. In this method, the PHB nanobeads were initially functionalized with a generic antibody (CD9) and dispersed in sample solution to capture bulk exosomes. After magnetic capture and purification, exosome-bound PHB nanobeads are transferred to CA125 antibody-modified, screen-printed electrodes. The peroxidase activity of HRP via the H_2O_2/HRP/HQ redox cycling system was then used to achieve an electrochemical quantification of CA125-specific exosomes present in the cell solution. (B) Amperometric responses for the detection of exosomes in the presence (red) and absence (no template control/NoT) of 10^7 particles/mL in a buffer. (C) Corresponding current densities for the target (right bar) and control (left bar) samples. (D) Current density for the designated concentration of exosomes extracted from the OVCAR3 cell line. The concentration varies between 10^3 and 10^7 particles/mL. (E) Corresponding bar diagram. (F,G) Comparative analysis of exosomes extracted from the ovarian cancer cell line and a normal cell line (Met-5A). (F) Amperometric response for different cell lines and (G) corresponding bar diagram representing current density comparison between different cell lines. Each data point represents the average of three repeat trails, and error bars represent the standard deviation of measurements (%RSD = <5%, for n = 3).

subsequently enables target adsorption/hybridization on the electrode surface.

A relative standard deviation (%RSD) for three independent measurements was estimated to be <5.0%, indicating a good reproducibility of assay toward the detection and quantification of DNA methylation levels. The lower limit of detection and the reproducibility of the assay over a wide range of methylation levels with low input DNA amounts demonstrated the applicability of PHB nanobeads as dispersible capture agents for isolating and purifying DNA targets.

3.5. Analysis of DNA Methylation Levels in Plasma Samples. To demonstrate the application of our superparamagnetic PHB nanobead-based electrochemical assay for detection of methylated DNA in a complex biological matrix, we compared the current density responses of various DNA methylation levels in complex human plasma (Figure 4D,E).

https://doi.org/10.1021/acsami.1c05355
ACS Appl. Mater. Interfaces 2021, 13, 31418−31430

Figure 4D,E shows that the observed current density responses enabled a linear dynamic range from 5 to 100% DNA methylation with an R^2 value of 0.9836. As compared to the buffer samples, the current density responses in plasma showed a decrease at the same % DNA methylation. This may be a result of the complexity of the plasma sample, which contains excessive background of nontarget biomolecules that have the potential to interfere via nonspecific binding during capture and isolation steps and also through nonspecific adsorption on the sensor platform during the detection process. A DNA methylation level as low as 5% could be detected for 10 ng of input DNA and indicated that our assay is effective for the isolation and detection of low methylated DNA levels in untreated/undiluted human plasma.

The detection sensitivity of 5% methylation obtained in plasma samples remains similar to the prior set of experiments performed in a buffer (Figure 4B,C). This highlighted the utility of our bioengineered superparamagnetic Fe_3-Z_6-PHB nanobeads in magnetic isolation of methylated DNA targets in human plasma. It is also worth noting that the obtained lowest detectable level of 5% methylation in plasma was superior to that of previously reported DNA methylation electrochemical assays using SPEs[47−49] but does not require any use of bisulfite treatment or PCR amplification during the assay, which could alter original methylation levels in samples.

3.6. Analysis of Global DNA Methylation Levels in Ovarian Cancer Cells. To further investigate the applicability of our superparamagnetic Fe_3-Z_6-PHB nanobead-based electrochemical assay for accurately detecting methylation levels in different cancer cells, extracted DNAs derived from ovarian cancer cell lines (SKOV3 and OVCAR3) and a noncancerous cell line (MeT-5A) were tested (Figure 4F,G). A fully unmethylated (0% methylated) WGA DNA and a fully methylated (100% methylated) Jurkat DNA were used as internal standards. We observed varying current density responses for the different samples, thereby indicating different levels of DNA methylation. The current density responses for SKOV3 and OVCAR3 were significantly high (35.6 and 28.5 μA cm^{-2}) as compared to WGA (2.27 μA cm^{-2}) and suggested that global DNA methylation levels in SKOV3 and OVCAR3 are higher. These findings are in agreement with previously reported global methylation levels in ovarian cancer cell lines.[50] This cell line data also shows good interassay reproducibility (%RSD of <4.63% for n = 3) for analyzing DNA methylation levels in ovarian cancer cell lines.

The developed superparamagnetic Fe_3-Z_6-PHB nanobead-based electrochemical assay offers several benefits such as the use of inexpensive disposable SPE-Au electrodes, which could allow low-cost analysis of DNA methylation. In addition, it allows rapid and efficient isolation and purification of methylated DNA targets without the need for traditional tedious and prolonged target purification workflows from cancer cells. Fe_3-Z_6-PHB nanobeads could be modified for specific target recognition and may be reusable for lower assay cost. The avoidance of bisulfite treatment and direct adsorption of methylated DNA targets onto the electrode surface for electrochemical detection are unique for simplifying the assay protocol and do not require any electrode surface premodification steps.

3.7. Application of PHB Nanobeads for Isolation and Detection of Exosomes. Figure 5A shows an electrochemical exosome assay principle using superparamagnetic Fe_3-Z_6-PHB nanobeads. First, CD9−HRP superparamagnetic nanobead complexes were added and dispersed into samples containing exosome targets. The generic CD9 antibodies specifically recognize and bind to exosomes. The exosome targets bound to the superparamagnetic PHB nanobeads were then magnetically isolated and eluted from the nanobeads by lowering the pH of glycine to 2.7. Purified CD9−HRP-bound exosomes were obtained after nanobeads were removed via magnetic attraction. Lastly, the CD9−HRP-bound exosome targets were adsorbed onto CA125 antibody-modified, screen-printed electrodes and electrochemically quantified by measuring the cathodic current generated by the enzymatic reduction of H_2O_2 mediated by HQ. This current is proportional to the amount of exosomes present. To check the functionality of the assay, we investigated the assay performance in the presence and absence of an exosome target. Figure 5C shows an 11-fold higher current density response for exosomes compared to the negative control (0.82 vs 0.07 μA cm^{-2}).

As exosomes are secreted by both normal and cancer cells, increasing studies have shown that cancer cells secrete a larger number of exosomes compared to normal cells, and this number is relative to the stage of cancer. Thus, at early stages of cancer, the number of exosomes from disease-specific cells could be very low, which potentially presents challenges for their isolation and detection. Hence, it is imperative to develop highly sensitive methods. The sensitivity of the assay was assessed by measuring the serial dilutions of exosomes derived from ovarian cancer cell line samples ranging from 10^3 to 10^7 exosomes/mL. As shown in Figure 5D, the amperometric current density response increased with the increasing target exosome concentration. As the amount of the surface-attached cancer-specific exosomes is proportional to the amount of the attached cancer-related antibodies, the higher the amount of exosomes, the higher the current signal generated at the glassy carbon electrode is. The linear regression equation was found to be y (μA cm^{-2}) = 0.146x − 0.118, with a correlation coefficient (R^2) of 0.969. The relative standard deviation of three independent measurements was estimated to be <5% indicating good reproducibility of the platform. The assay achieved an LOD of 10^3 exosomes/mL, which is comparable to our previous study based on engineered inorganic superparamagnetic nanoparticles (gold-loaded nanoporous ferric oxide).[51] It is worth noting that our assay achieved a higher sensitivity compared to recent reports using surface plasmon resonance and microfluidics-based exosome analysis techniques.[52,53]

To check the specificity of the assay, control experiments were conducted. In a positive control experiment, exosomes (i.e., 10^7 exosomes/mL) derived from ovarian cancer cell line (OVCAR3) extracts were initially captured by CD9 antibody-functionalized magnetic nanobeads, which were subpopulated by the biotinylated CA125 antibody. As depicted in Figure 5F, a significant current density response was observed for the ovarian cancer-specific exosomes in OVCAR3 cell extracts. As a negative control, 10^7 exosomes/mL derived from a noncancerous cell line (MeT-5A) were tested using the biotinylated CA125 antibody. Since the CA125 antibody is not specific to ovarian cancer exosomes, no amperometric current response for ovarian cancer-specific exosomes was expected. However, we observed a lower current density response compared to that of the positive control (0.31 vs 0.83 μA cm^{-2}). This may be a result of the nonspecific adsorption of the functionalized CA125 antibody on the sensor surface.

https://doi.org/10.1021/acsami.1c05355
ACS Appl. Mater. Interfaces 2021, 13, 31418−31430

4. DISCUSSION

We have bioengineered and assembled superparamagnetic PHB nanobeads for isolation and electrochemical detection of both methylated DNA and exosome cancer biomarkers. The PHB nanobeads were produced in engineered *E. coli*, a bacterium used for industrial production of protein-based products and biopolymers.[3] Cost-effective manufacturing, stability (up to 95 °C, pH range of 2−12), and oriented high-density display of protein functions make PHB nanobeads attractive for uses as a biosensor in single-use applications.[14,39] Designed PHB nanobeads were manufactured and characterized to assess their composition, size distribution, zeta potential, antibody-binding capacity, and superparamagnetism.

A process was devised to utilize the surface-embedded iron oxide-binding peptides to bind colloidal iron oxide to obtain magnetic properties while retaining the antibody-binding capability. Superparamagnetic PHB nanobeads were biochemically and physically characterized. The performance as capture resins was assessed by characterizing magnetic and specific binding properties in the electrochemical detection assay such as methylated DNA recognition mediated by the bound HRP−antibody conjugate. After magnetic isolation of methylated DNA targets, electrochemical target quantification was achieved by direct adsorption of the eluted methylated DNA on an SPE-Au surface and by amperometry using a catalytic redox cycling system of H_2O_2/HRP/HQ. Sensitive and specific detection of DNA methylation in genomic DNA is important for rapid epigenetic evaluations. We achieved a high analytical performance (LOD = 5% DNA methylation, %RSD $\leq$ 5.0) in human plasma matrices and cancer cell lines. The elimination of capture probes, hybridization steps, radioactive labels, methylation-sensitive restriction enzymes, and sequencing analysis simplifies our assay. The utility of superparamagnetic PHB nanobeads was further demonstrated by CD9 antibody-mediated specific capture of cancer cell-derived exosomes. These exosomes were eluted from the nanobeads, which were subsequently removed by magnetic separation. Purified exosomes were quantified by electrochemical detection providing means for cancer diagnostics. N.B., the superparamagnetic PHB nanobeads are conceivable to serve as bioseparation resin for large-scale batch-mode purification of exosomes, which increasingly attract interest not only as diagnostics markers but also for uses as therapeutics. The current gold standard method for exosome isolation based on differential centrifugation requires centrifugation of up to 120,000*g*.[54] This method is tedious and time-consuming (>10). With sample volumes as low as 5 μL, our assay generated an electrochemical signal within 2 h. Compared to other methods previously reported, our assay exhibits advantages of ease of operation, low cost, specificity, and sensitivity. With a linear response spanning over four orders of magnitude, we achieved a sensitive electrochemical detection of exosomes with an LOD of 10^3 exosomes/mL. Considering the great importance of exosome-mediated signal transmission among cells, our assay may present an important step toward the construction of a simple biosensor that can detect exosomes in complex media. Given that the PHB nanobead surface can be readily tuned for efficient isolation and electrochemical detection of different targets, we envisage that the developed superparamagnetic PHB nanobead-based electrochemical assay offers a versatile diagnostic platform for specific and sensitive detection of a range of disease biomarkers, i.e., enabling diagnosis of various diseases.

■ ASSOCIATED CONTENT

Supporting Information

The Supporting Information is available free of charge at https://pubs.acs.org/doi/10.1021/acsami.1c05355.

Protein concentration and PHB nanobead yield (Figure S1); TEM images of various PHB nanobeads (Figure S2); human IgG-binding capacity of PHB nanobeads displaying ZZ and Fe domains without and with a ferrofluid (Figure S3); electrochemical detection of methylated DNA in a buffer sequestered by engineered superparamagnetic PHB nanobeads (Figure S4); amperometric response for PHB, Z_6-PHB, and Fe_3-Z_6-PHB nanobeads to detect 100% methylated DNA sequences (Figure S5); description of bacterial strains, plasmids, and primers used in this study (Table S1); MS-Q-TOF analysis of PHB and PHB-fusion proteins (Table S2); particle size and zeta potential measurements (Table S3) (PDF)

■ AUTHOR INFORMATION

Corresponding Authors

Muhammad J. A. Shiddiky − *School of Environment and Science and Queensland Micro- and Nanotechnology Centre (QMNC), Griffith University, Nathan, Queensland 4111, Australia;* orcid.org/0000-0003-4526-4109; Phone: +61(07) 373 59617; Email: m.shiddiky@griffith.edu.au

Bernd H. A. Rehm − *Centre for Cell Factories and Biopolymers (CCFB), Griffith Institute for Drug Discovery, Griffith University, Nathan, Queensland 4111, Australia; Menzies Health Institute Queensland (MHIQ), Griffith University, Gold Coast, Queensland 4222, Australia;* orcid.org/0000-0003-3908-8903; Phone: +61466024339; Email: b.rehm@griffith.edu.au

Authors

Narshone Soda − *School of Environment and Science and Queensland Micro- and Nanotechnology Centre (QMNC), Griffith University, Nathan, Queensland 4111, Australia;* orcid.org/0000-0002-1921-7176

Zennia Jean Gonzaga − *School of Environment and Science and Centre for Cell Factories and Biopolymers (CCFB), Griffith Institute for Drug Discovery, Griffith University, Nathan, Queensland 4111, Australia*

Shuxiong Chen − *Centre for Cell Factories and Biopolymers (CCFB), Griffith Institute for Drug Discovery, Griffith University, Nathan, Queensland 4111, Australia*

Kevin M. Koo − *The University of Queensland Centre for Clinical Research (UQCCR), Herston, Queensland 4029, Australia*

Nam-Trung Nguyen − *Queensland Micro- and Nanotechnology Centre (QMNC), Griffith University, Nathan, Queensland 4111, Australia*

Complete contact information is available at: https://pubs.acs.org/10.1021/acsami.1c05355

Author Contributions

#N.S. and Z.J.G. contributed equally as cofirst authors. M.J.A.S. and B.H.A.R. are equal senior authors. All authors have given

approval to the final version of the manuscript. M.J.A.S. and B.H.A.R. conceived the project; N.S., Z.J.G., S.C., and K.M.K. designed and performed the experiments and analyzed data; N.S. and Z.J.G. wrote the manuscript; N.-T.N. provided scientific inputs; M.J.A.S. and B.H.A.R. revised the manuscript and supervised the entire project.

Notes

The authors declare no competing financial interest.

■ ACKNOWLEDGMENTS

The authors acknowledge the facilities and the scientific and technical assistance of the Australian Microscopy & Microanalysis Research Facility at the Centre for Microscopy and Microanalysis, as well as the Centre for Clinical Research and the Metabolomics Australia−Queensland Node at the University of Queensland. B.H.A.R. acknowledges support from the Australian Research Council (ARC) Discovery Project (DP200100874) and the ARC Linkage Infrastructure, Equipment and Facilities (LE20010014).

■ REFERENCES

(1) Lee, G.-H.; Moon, H.; Kim, H.; Lee, G. H.; Kwon, W.; Yoo, S.; Myung, D.; Yun, S. H.; Bao, Z.; Hahn, S. K. Multifunctional materials for implantable and wearable photonic healthcare devices. *Nat. Rev. Mater.* **2020**, *5*, 149−165.

(2) Park, S.-m.; Aalipour, A.; Vermesh, O.; Yu, J. H.; Gambhir, S. S. Towards clinically translatable *in vivo* nanodiagnostics. *Nat. Rev. Mater.* **2017**, *2*, 17014.

(3) Moradali, M. F.; Rehm, B. H. A. Bacterial biopolymers: from pathogenesis to advanced materials. *Nat. Rev. Microbiol.* **2020**, *18*, 195−210.

(4) Sawant, S. N. 13 - Development of Biosensors From Biopolymer Composites. In *Biopolymer Composites in Electronics*; Sadasivuni, K. K.; Ponnamma, D.; Kim, J.; Cabibihan, J. J.; AlMaadeed, M. A. Eds.; Elsevier, 2017, pp. 353−383, DOI: 10.1016/B978-0-12-809261-3.00013-9.

(5) Fahmy, S. A.; Alawak, M.; Brüßler, J.; Bakowsky, U.; El Sayed, M. M. H. Nanoenabled bioseparations: current developments and future prospects. *BioMed Res. Int.* **2019**, *2019*, 4983291.

(6) Arias, L. S.; Pessan, J. P.; Vieira, A. P. M.; de Lima, T. M. T.; Delbem, A. C. B.; Monteiro, D. R. Iron Oxide Nanoparticles for Biomedical Applications: A Perspective on Synthesis, Drugs, Antimicrobial Activity, and Toxicity. *Antibiotics* **2018**, *7*, 46.

(7) Rehm, B. H. A. Biogenesis of microbial polyhydroxyalkanoate granules: a platform technology for the production of tailor-made bioparticles. *Curr. Issues Mol. Biol.* **2007**, *9*, 41−62.

(8) Parlane, N. A.; Gupta, S. K.; Rubio-Reyes, P.; Chen, S.; Gonzalez-Miro, M.; Wedlock, D. N.; Rehm, B. H. A. Self-Assembled Protein-Coated Polyhydroxyalkanoate Beads: Properties and Biomedical Applications. *ACS Biomater. Sci. Eng.* **2017**, *3*, 3043−3057.

(9) Grage, K.; McDermott, P.; Rehm, B. H. A. Engineering *Bacillus megaterium* for production of functional intracellular materials. *Microb. Cell Fact.* **2017**, *16*, 211.

(10) Jahns, A. C.; Haverkamp, R. G.; Rehm, B. H. A. Multifunctional Inorganic-Binding Beads Self-Assembled Inside Engineered Bacteria. *Bioconjugate Chem.* **2008**, *19*, 2072−2080.

(11) Peters, V.; Rehm, B. H. A. Protein engineering of streptavidin for in vivo assembly of streptavidin beads. *J. Biotechnol.* **2008**, *134*, 266−274.

(12) Ogura, K.; Rehm, B. H. A. Alginate Encapsulation of Bioengineered Protein-Coated Polyhydroxybutyrate Particles: A New Platform for Multifunctional Composite Materials. *Adv. Funct. Mater.* **2019**, *29*, 1901893.

(13) Rehm, B. H. A.; Steinbüchel, A. Biochemical and genetic analysis of PHA synthases and other proteins required for PHA synthesis. *Int. J. Biol. Macromol.* **1999**, *25*, 3−19.

(14) Grage, K.; Jahns, A. C.; Parlane, N.; Palanisamy, R.; Rasiah, I. A.; Atwood, J. A.; Rehm, B. H. A. Bacterial Polyhydroxyalkanoate Granules: Biogenesis, Structure, and Potential Use as Nano-/Micro-Beads in Biotechnological and Biomedical Applications. *Biomacromolecules* **2009**, *10*, 660−669.

(15) Evert, B.; Vezina, B.; Rehm, B. H. A. Catalytically Active Bioseparation Resin Utilizing a Covalent Intermediate for Tagless Protein Purification. *ACS Appl. Bio Mater.* **2020**, 8911.

(16) Lewis, J. G.; Rehm, B. H. A. ZZ polyester beads: An efficient and simple method for purifying IgG from mouse hybridoma supernatants. *J. Immunol. Methods* **2009**, *346*, 71−74.

(17) Marques, C. R.; Wibowo, D.; Rubio-Reyes, P.; Serafim, L. S.; Soares, A. M. V. M.; Rehm, B. H. A. Bacterially assembled biopolyester nanobeads for removing cadmium from water. *Water Res.* **2020**, *186*, 116357.

(18) Koo, K. M.; Soda, N.; Shiddiky, M. J. A. Magnetic nanomaterial−based electrochemical biosensors for the detection of diverse circulating cancer biomarkers. *Curr. Opin. Electrochem.* **2021**, *25*, 100645.

(19) Heyn, H.; Esteller, M. DNA methylation profiling in the clinic: applications and challenges. *Nat. Rev. Genet.* **2012**, *13*, 679−692.

(20) Herman, J. G.; Baylin, S. B. Gene silencing in cancer in association with promoter hypermethylation. *N. Engl. J. Med.* **2003**, *349*, 2042−2054.

(21) Robertson, K. D.; Jones, P. A. DNA methylation: past, present and future directions. *Carcinogenesis* **2000**, *21*, 461−467.

(22) Rao, B. S.; Buckler-White, A. Direct visualization of site-specific and strand-specific DNA methylation patterns in automated DNA sequencing data. *Nucleic Acids Res.* **1998**, *26*, 2505−2507.

(23) Razin, A.; Cedar, H. DNA methylation and gene expression. *Microbiol. Rev.* **1991**, *55*, 451−458.

(24) Xuan, J.; Yu, Y.; Qing, T.; Guo, L.; Shi, L. Next-generation sequencing in the clinic: promises and challenges. *Cancer Lett.* **2013**, *340*, 284−295.

(25) Xiong, Z.; Laird, P. W. COBRA: a sensitive and quantitative DNA methylation assay. *Nucleic Acids Res.* **1997**, *25*, 2532−2534.

(26) Théry, C.; Zitvogel, L.; Amigorena, S. Exosomes: composition, biogenesis and function. *Nat. Rev. Immunol.* **2002**, *2*, 569−579.

(27) Théry, C. Exosomes: secreted vesicles and intercellular communications. *F1000 Biol. Rep.* **2011**, *3*, 15.

(28) Boriachek, K.; Islam, M. N.; Möller, A.; Salomon, C.; Nguyen, N.-T.; Hossain, M. S. A.; Yamauchi, Y.; Shiddiky, M. J. A. Biological Functions and Current Advances in Isolation and Detection Strategies for Exosome Nanovesicles. *Small* **2018**, *14*, 1702153.

(29) De Toro, J.; Herschlik, L.; Waldner, C.; Mongini, C. Emerging roles of exosomes in normal and pathological conditions: new insights for diagnosis and therapeutic applications. *Front. Immunol.* **2015**, *6*, 203.

(30) Sambrook, J.; Fritsch, E. F.; Maniatis, T. *Molecular cloning: a laboratory manual*; Cold spring harbor laboratory press, 1989.

(31) Jahns, A. C.; Maspolim, Y.; Chen, S.; Guthrie, J. M.; Blackwell, L. F.; Rehm, B. H. A. *In vivo* self-assembly of fluorescent protein microparticles displaying specific binding domains. *Bioconjugate Chem.* **2013**, *24*, 1314−1323.

(32) Amara, A. A.; Rehm, B. H. A. Replacement of the catalytic nucleophile cysteine-296 by serine in class II polyhydroxyalkanoate synthase from *Pseudomonas aeruginosa*-mediated synthesis of a new polyester: identification of catalytic residues. *Biochem. J.* **2003**, *374*, 413−421.

(33) Reyes, P. R.; Parlane, N. A.; Wedlock, D. N.; Rehm, B. H. A. Immunogencity of antigens from *Mycobacterium tuberculosis* self-assembled as particulate vaccines. *Int. J. Med. Microbiol.* **2016**, *306*, 624−632.

(34) Spiekermann, P.; Rehm, B. H. A.; Kalscheuer, R.; Baumeister, D.; Steinbüchel, A. A sensitive, viable-colony staining method using Nile red for direct screening of bacteria that accumulate polyhydroxyalkanoic acids and other lipid storage compounds. *Arch. Microbiol.* **1999**, *171*, 73−80.

(35) de Souza Pinto Lemgruber, R.; Valgepea, K.; Tappel, R.; Behrendorff, J. B.; Palfreyman, R. W.; Plan, M.; Hodson, M. P.; Simpson, S. D.; Nielsen, L. K.; Köpke, M.; Marcellin, E. Systems-level engineering and characterisation of *Clostridium autoethanogenum* through heterologous production of poly-3-hydroxybutyrate (PHB). *Metab. Eng.* **2019**, *53*, 14−23.
(36) Yalcin, S.; Khodadust, R.; Unsoy, G.; Ceren Garip, I.; Didem Mumcuoglu, Z.; Gunduz, U. Synthesis and Characterization of Polyhydroxybutyrate Coated Magnetic Nanoparticles: Toxicity Analyses on Different Cell Lines. *Synth. React. Inorg., Met.-Org., Nano-Met. Chem.* **2015**, *45*, 700−708.
(37) Hay, I. D.; Hooks, D. O.; Rehm, B. H. A. Use of bacterial polyhydroxyalkanoates in protein display technologies. In *Hydrocarbon and lipid microbiology protocols*; Springer, 2014; pp. 71−86, DOI: 10.1007/8623_2014_34.
(38) Koo, K. M.; Sina, A. A. I.; Carrascosa, L. G.; Shiddiky, M. J. A.; Trau, M. DNA−bare gold affinity interactions: mechanism and applications in biosensing. *Anal. Methods* **2015**, *7*, 7042−7054.
(39) Peters, V.; Rehm, B. H. A. *In Vivo* Enzyme Immobilization by Use of Engineered Polyhydroxyalkanoate Synthase. *Appl. Environ. Microbiol.* **2006**, *72*, 1777−1783.
(40) Rehm, B. H. A. Bacterial polymers: biosynthesis, modifications and applications. *Nat. Rev. Microbiol.* **2010**, *8*, 578−592.
(41) Draper, J. L.; Rehm, B. H. Engineering bacteria to manufacture functionalized polyester beads. *Bioengineered* **2012**, *3*, 203−208.
(42) Mifune, J.; Grage, K.; Rehm, B. H. A. Production of Functionalized Biopolyester Granules by Recombinant *Lactococcus lactis*. *Appl. Environ. Microbiol.* **2009**, *75*, 4668−4675.
(43) Ito, A.; Shinkai, M.; Honda, H.; Kobayashi, T. Medical application of functionalized magnetic nanoparticles. *J. Biosci. Bioeng.* **2005**, *100*, 1−11.
(44) González-Miró, M.; Rodríguez-Noda, L. M.; Fariñas-Medina, M.; Cedré-Marrero, B.; Madariaga-Zarza, S.; Zayas-Vignier, C.; Hernández-Cedeño, M.; Kleffmann, T.; García-Rivera, D.; Vérez-Bencomo, V.; Rehm, B. H. A. Bioengineered polyester beads co-displaying protein and carbohydrate-based antigens induce protective immunity against bacterial infection. *Sci. Rep.* **2018**, *8*, 1888−1815.
(45) Turker, M. S. Gene silencing in mammalian cells and the spread of DNA methylation. *Oncogene* **2002**, *21*, 5388−5393.
(46) Haque, M. H.; Gopalan, V.; Yadav, S.; Islam, M. N.; Eftekhari, E.; Li, Q.; Carrascosa, L. G.; Nguyen, N.-T.; Lam, A. K.; Shiddiky, M. J. A. Detection of regional DNA methylation using DNA-graphene affinity interactions. *Biosens. Bioelectron.* **2017**, *87*, 615−621.
(47) Koo, K. M.; Sina, A. A. I.; Carrascosa, L. G.; Shiddiky, M. J. A.; Trau, M. eMethylsorb: rapid quantification of DNA methylation in cancer cells on screen-printed gold electrodes. *Analyst* **2014**, *139*, 6178−6184.
(48) Haque, M. H.; Gopalan, V.; Islam, M. N.; Masud, M. K.; Bhattacharjee, R.; Hossain, M. S. A.; Nguyen, N.-T.; Lam, A. K.; Shiddiky, M. J. A. Quantification of gene-specific DNA methylation in oesophageal cancer via electrochemistry. *Anal. Chim. Acta* **2017**, *976*, 84−93.
(49) Koo, K. M.; Wee, E. J. H.; Rauf, S.; Shiddiky, M. J. A.; Trau, M. Microdevices for detecting locus-specific DNA methylation at CpG resolution. *Biosens. Bioelectron.* **2014**, *56*, 278−285.
(50) Bhattacharjee, R.; Moriam, S.; Nguyen, N.-T.; Shiddiky, M. J. A. A bisulfite treatment and PCR-free global DNA methylation detection method using electrochemical enzymatic signal engagement. *Biosens. Bioelectron.* **2019**, *126*, 102−107.
(51) Boriachek, K.; Masud, M. K.; Palma, C.; Phan, H.-P.; Yamauchi, Y.; Hossain, M. S. A.; Nguyen, N.-T.; Salomon, C.; Shiddiky, M. J. A. Avoiding Pre-Isolation Step in Exosome Analysis: Direct Isolation and Sensitive Detection of Exosomes Using Gold-Loaded Nanoporous Ferric Oxide Nanozymes. *Anal. Chem.* **2019**, *91*, 3827−3834.
(52) Sina, A. A. I.; Vaidyanathan, R.; Dey, S.; Carrascosa, L. G.; Shiddiky, M. J. A.; Trau, M. Real time and label free profiling of clinically relevant exosomes. *Sci. Rep.* **2016**, *6*, 30460.
(53) Zhao, Z.; Yang, Y.; Zeng, Y.; He, M. A microfluidic ExoSearch chip for multiplexed exosome detection towards blood-based ovarian cancer diagnosis. *Lab Chip* **2016**, *16*, 489−496.
(54) Tauro, B. J.; Greening, D. W.; Mathias, R. A.; Ji, H.; Mathivanan, S.; Scott, A. M.; Simpson, R. J. Comparison of ultracentrifugation, density gradient separation, and immunoaffinity capture methods for isolating human colon cancer cell line LIM1863-derived exosomes. *Methods* **2012**, *56*, 293−304.

https://doi.org/10.1021/acsami.1c05355
ACS Appl. Mater. Interfaces 2021, 13, 31418−31430